Lead-position dependent regular oscillations and random fluctuations of conductance in graphene quantum dots

2013 J. Phys.: Condens. Matter 25 085502

(http://iopscience.iop.org/0953-8984/25/8/085502)

J. Phys.: Condens. Matter **25** (2013) 085502 (9pp) doi:10.1088/0953-8984/25/8/085502

Lead-position dependent regular oscillations and random fluctuations of conductance in graphene quantum dots

Liang Huang[1,2], Rui Yang[2], Ying-Cheng Lai[2,3] and David K Ferry[2,3,4]

[1] Institute of Computational Physics and Complex Systems and Key Laboratory for Magnetism and Magnetic Materials of MOE, Lanzhou University, Lanzhou, Gansu 730000, People's Republic of China
[2] School of Electrical, Computer, and Energy Engineering, Arizona State University, Tempe, AZ 85287, USA
[3] Department of Physics, Arizona State University, Tempe, AZ 85287, USA
[4] Center for Solid State Electronics Research, Arizona State University, Tempe, AZ 85287, USA

E-mail: huangl@lzu.edu.cn

Received 30 September 2012, in final form 7 December 2012
Published 23 January 2013
Online at stacks.iop.org/JPhysCM/25/085502

Abstract
Quantum interference causes a wavefunction to have sensitive spatial dependence, and this has a significant effect on quantum transport. For example, in a quantum-dot system, the conductance can depend on the lead positions. We investigate, for graphene quantum dots, the conductance variations with the lead positions. Since for graphene the types of boundaries, e.g., zigzag and armchair, can fundamentally affect the quantum transport characteristics, we focus on rectangular graphene quantum dots, for which the effects of boundaries can be systematically studied. For both zigzag and armchair horizontal boundaries, we find that changing the positions of the leads can induce significant conductance variations. Depending on the Fermi energy, the variations can be either regular oscillations or random conductance fluctuations. We develop a physical theory to elucidate the origin of the conductance oscillation/fluctuation patterns. In particular, quantum interference leads to standing-wave-like-patterns in the quantum dot which, in the absence of leads, are regulated by the energy-band structure of the corresponding vertical graphene ribbon. The observed 'coexistence' of regular oscillations and random fluctuations in the conductance can be exploited for the development of graphene-based nanodevices.

(Some figures may appear in colour only in the online journal)

1. Introduction

Graphene, a single layer of carbon atoms arranged in a honeycomb lattice, has attracted much recent interest [1]. Potential applications of graphene range from electronics to nano- biosensors. For example, due to the distinctly high mobility of the charge carriers in graphene [2], nanoscale electronic devices made of graphene, such as p–n junctions and transistors, can be superior to their Si-based counterparts [3]. Other applications include spintronics [4], flexible and transparent photonic devices [5, 6], vapor molecular sensors [7], DNA sequencing [8], single-bacterium resolution biodevice and DNA transistor [9], and cellular interfaces for electrical recording of cell membrane activities [10], etc. For any application, there is a need to connect the graphene device to external voltage or current source via metal leads. Ideally, there should be zero resistance between the metal lead and the graphene. However, experiments have shown that the contact resistance can approach or even exceed the quantum resistance [11, 12]. This indicates that some form of injection barrier must exist at the metal–graphene interface, restricting the transmitting modes to be a few [11–15].

A useful setting to study the effect of contact on transport is graphene quantum dots where the leads are assumed to be ideal but they are narrow and can only support a few

transverse modes [16]. This setup can also be used to explore the transport properties of quantum point contacts (QPCs), which in general depend on the geometry of the structure [15, 17]. A basic geometric parameter is the relative position of the lead (or QPC) to the graphene device, which can affect the conductance significantly. To develop graphene-based device for applications, it is of paramount interest to understand how the conductance changes as a function of the lead position. This effect has been noted previously in the contexts of semiconductor–superconductor microjunctions [18] and transport through evanescent waves in graphene quantum dots [19]. Because of intervalley scattering the conductance fluctuation could be sample- and geometry-dependent [20].

In a recent Letter [21], we studied a simple rectangle graphene quantum dot with narrow leads and zigzag horizontal boundaries, and found that, depending on the Fermi energy, there are periodic conductance oscillations and random conductance fluctuations when the lead position is varied systematically. These oscillations are related to the change in the band structure that is induced by the edge of the graphene dot, where the bands are restructured into bonding and antibonding surface bands. We have briefly discussed that the periodic conductance oscillations are caused by the bonding bands, where the phases of the two atoms in a unit cell are identical. Antibonding bands, where the phases of the two atoms have a π difference, do not contribute to the conductance. Similar interference pattern has also been observed by Gonzalez *et al* in [22].

The purpose of this paper is to investigate the effect of distinct graphene boundaries, i.e., zigzag and armchair, on the lead-position dependent conductance variations. Intuitively, if the lead is located in a region where the local density of states (LDOS) is low, electrons can hardly hop out of the localized pattern to get into the lead, resulting in a small conductance value [23]. Opposite situations can occur when the lead is in a different region, leading to a large conductance. Our systematic computations with varying lead positions reveal significant conductance fluctuations. A physical analysis indicates that the fluctuations are caused by various standing-wave patterns in the quantum dot. In particular, the wavevector of the wavefunction follows the underlying dispersion relation. For tall and narrow quantum dots, the relation can be approximated by the dispersion relation of the corresponding graphene ribbon when viewed vertically in the absence of the leads, as shown in figure 1. There are two atoms in a unit cell (denoted by A and B), representing a pseudo-spin of the system. The wavefunction thus typically has a phase difference for the two atoms. If the horizontal boundary is zigzag, the ribbon has armchair boundary in the vertical direction, and there are two sets of bands. At the bottom of these bands, for one set, the wavefunctions for A atom have the same phase as that for B atom in the same unit cell (bonding), e.g., the value of the wavefunction for A and B atoms are the same. For the other set, the wavefunctions for A atoms have the opposite value as that for B atoms (antibonding), which do not contribute to the transmission. While for armchair graphene quantum dots, the vertical graphene ribbon is zigzag, whose bands

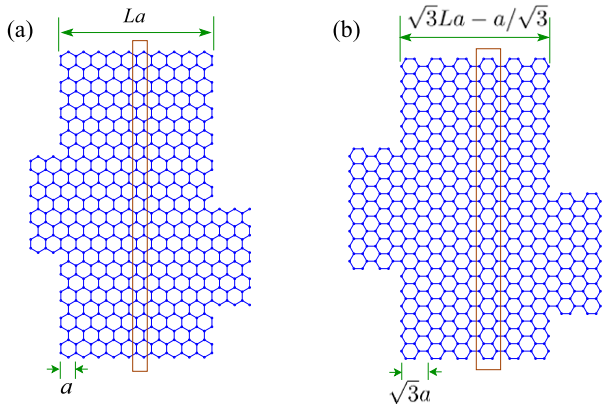

Figure 1. A schematic illustration of rectangular graphene quantum dots with zigzag horizontal boundaries (a) and armchair horizontal boundaries (b), where the left and right leads are semi-infinite. Because of the lattice structure, the position of the lead can only be changed vertically in a multiple of the lattice distance, which is $\sqrt{3}a$ for (a) and a for (b), where $a = 0.246$ nm is the lattice constant. We have $i_{\mathrm{L/R}} = 1$ if the left/right lead resides at the bottom of the dot. The rectangles indicate a layer of N atoms, and L is the number of layers. The number of atoms in the device is about $N \times L$. In (a), the geometric parameters are $i_{\mathrm{L}} = 5$, $i_{\mathrm{R}} = 3$, $L = 10$, and $N = 12 \times 4$. In (b), the parameters are $i_{\mathrm{L}} = 7$, $i_{\mathrm{R}} = 4$, $L = 6$, and $N = 20 \times 4 + 2 = 82$.

do not have the bonding or antibonding properties. We note that in the nanotransport literature, conductance fluctuations are usually referred to those with respect to varying electron energy or changing magnetic field [24], the origin of which can generally be attributed to scarred or pointer states in the underlying dot structure. The fluctuations reported here are induced purely by geometrical variance in the whole device (quantum dot plus leads), caused by a different mechanism.

The organization of the rest of the paper is as follows. In section 2, we describe the model setup. In sections 3 and 4, we present systematic numerical results and physical analysis for graphene quantum dots with zigzag and armchair boundaries, respectively. Conclusions and a brief discussion are presented in section 5.

2. Graphene quantum-dot model

Figure 1 shows the setup of a rectangular graphene quantum dot where the vertical positions of the leads can be varied. We assume the leads are semi-infinite, narrow graphene ribbons supporting only a few transmission modes (8 in our simulation for both zigzag and armchair cases). The rectangular device can be divided into L slices, where each slice has N atoms so that the number of atoms in the device is about $N \times L$. The size of the device is much larger than the width of the leads. In realistic situations the positions of the leads can hardly be tuned precisely on the atomic scale. A goal of this paper is to investigate how this position inaccuracy affects the overall conductance of the device. To be specific, the position of the leads can vary only in an integer multiple of the basic lattice unit in the vertical direction. To capture the essential physics, we fix the left lead, systematically change

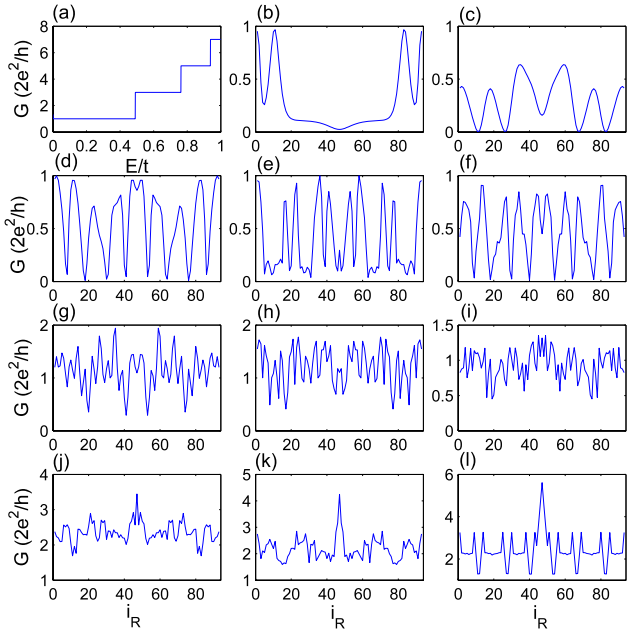

Figure 2. For a zigzag dot with $L = 20$ and $N = 96 \times 4$, (a) conductance versus Fermi energy, (b)–(l) conductance versus right lead position i_R for Fermi energy $E/t = 0, 0.1, 0.2, \ldots, 1$, respectively. The left lead is fixed at the middle of the dot: $i_L = 47$.

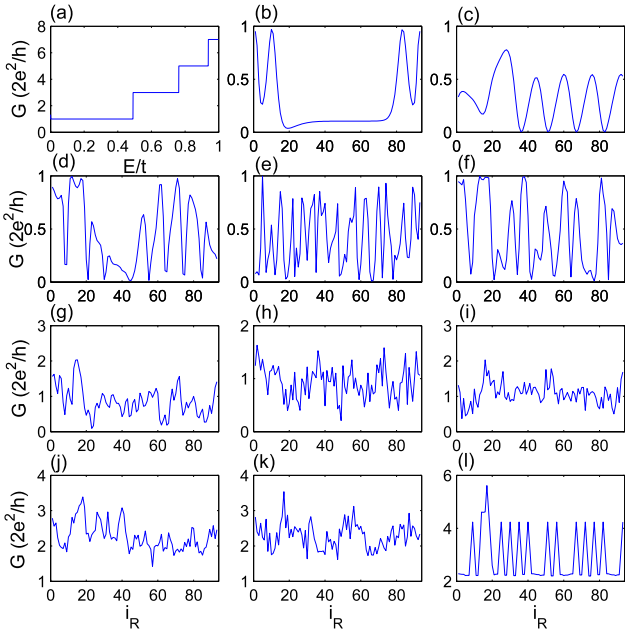

Figure 3. The same plots as figure 2 except $i_L = 17$.

the Fermi energy and the position of the right lead (denoted by i_R), and examine how the conductance changes with these parameters. We employ the tight-binding Hamiltonian and the standard Green's function formalism to calculate the coherent transmission. The Landauer formula can then be used to calculate the conductance [25, 26]. In the Hamiltonian, the nearest-neighbor hopping energy is $t \approx 2.8$ eV [1]. At low temperature the conductance is proportional to the transmission [25]. For a small quantum dot with well-defined shape and terminations, many-body effects such as Coulomb blockade can also be relevant to the conductance, which is neglected in this paper.

3. Graphene systems with zigzag horizontal boundary

Figure 2 shows, for a graphene dot with zigzag horizontal boundary, the conductance versus i_R for a set of fixed Fermi energies, where the device size is $L = 20$ and $N = 96 \times 4$, and the position of the left lead is fixed at $i_L = 47$ (the middle of the device). For this dot structure, i_R can be varied from 1 (bottom) to 93 (top). Panel (a) shows the conductance for an infinite graphene ribbon made of the leads. Thus for $E/t = 0, 0.1, \ldots, 0.4$ (corresponding to panels (b)–(f), respectively), there is at most one transmission mode in the lead, limiting the conductance to 1 in the unit of quanta $2e^2/h$. For $E/t = 0.5, 0.6, 0.7$ (panels (g)–(i), respectively), the maximum number of modes is 3, and for $E/t = 0.8, 0.9$ (panels (j) and (k), respectively), the maximum number of modes is 5, and when E/t equals 1, the number of modes supported by each lead is 8. From this set of results, we see that, for a given dot with the left lead fixed, the conductance depends sensitively on the position of the right lead. For a given energy, for some positions, the conductance can have large values ($\sim$1), while for some other positions, the conductance could be almost zero (in the order of 10^{-4}). This substantiates our conjecture that the conductance and therefore the performance of the device could be significantly influenced by placing the lead at different locations. Another observation is that for some energy values, the variation of the conductance versus the lead position seems to be periodic (figures 2(c)–(f)), while for other cases, it is more randomized (figures 2(i)–(k)). To see if the observed periodicity and randomness is persistent, we shift the left lead to $i_L = 17$, and show the results in figure 3. For some energy levels, the two cases, where the only difference is the position of the left lead, have some common patterns, e.g., they both are roughly periodic with the same period (panels (c)–(f) of figures 2 and 3) or both appear random (panels (i)–(k)). While for some other cases the behaviors are quite different (panels (g), (h)). These behaviors are quite robust, as we have verified by, for example, changing the width and thus the number of transverse modes of the leads, and the height and width of the dot.

To understand the periodic and random behaviors in the dependence of conductance on the lead position, we vary the energy continuously and generate a contour plot of the conductance versus the energy and lead position, as shown in figure 4, for both $i_L = 47$ (a), (b) and $i_L = 17$ (c), (d). For better visualization effect, the energy is separated into two intervals: $0 < E/t < 0.4905$ (figures 4(a) and (c)) where the conductance is supported by only one transmission mode in the leads, and $0.4905 < E/t < 1$ (figures 4(b) and (d)). We observe complicated conductance patterns. First, the number of transmission modes in the leads regulates the overall scale of the conductance variations, and the behavior appears quite different for $i_L = 47$ and $i_L = 17$ in spite of some common

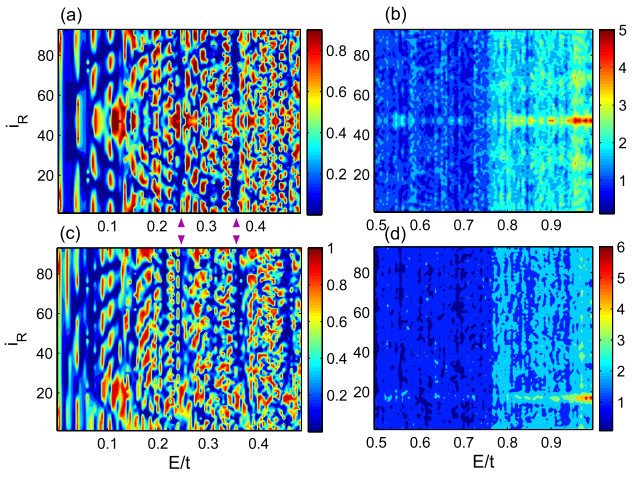

Figure 4. Contour plot of the conductance (in units of $2e^2/h$) on the i_R-E/t plane for $i_L = 47$ (a), (b) and $i_L = 17$ (c), (d). (a), (c) $0 < E/t < 0.4905$ where the maximum mode number is 1 and (b), (d) $0.4905 < E/t < 1$.

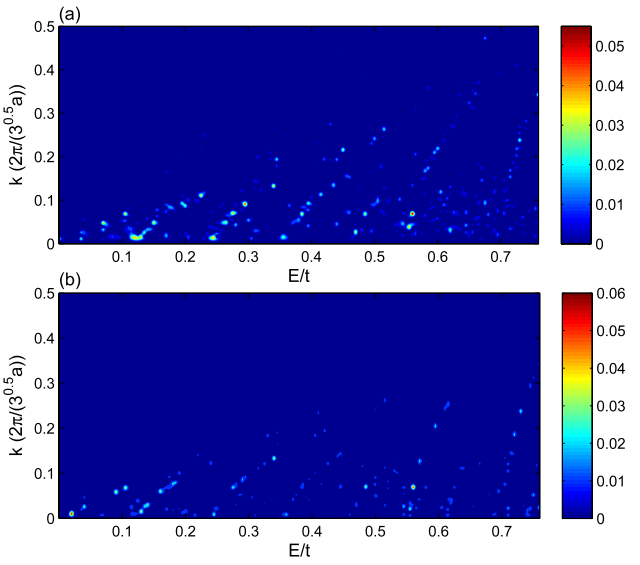

Figure 5. Contour plot of the power spectrum of the conductance variation $\widetilde{G}$ in the wavevector k (from i_R) and E/t plane for $i_L = 47$ (a) and $i_L = 17$ (b). The units are arbitrary for the power spectrum.

features. For example, for $E/t < 0.4905$, there is only one transmission mode, so the maximum conductance is one ($2e^2/h$). As E/t varies from 0.4905 to about 0.75, there are three transmission modes, and there are five transmission modes for $0.75 < E/t < 0.95$. This can also be seen from figures 4(b) and (d) as the abrupt changes in these transition values. Second, for each energy range where the number of the transmission modes is fixed, there are sub-energy intervals possessing similar conductance patterns, as marked in figure 4 by the arrows between figures 4(a) and (c). This sub-energy interval is independent of the position of the left lead. As we shall explain later, the presence of the sub-energy interval depends on the width L of the rectangular quantum dot. When the width varies, the range of this sub-energy interval also changes.

To gain further insight into the conductance pattern, at each given energy E, for the conductance curve $G(i_R, E)$ versus the right lead position i_R, we subtract the mean value $\langle G(\cdot, E)\rangle_{i_R}$ with respect to i_R to get the conductance variation $\widetilde{G}(i_R, E) = G(i_R, E) - \langle G(\cdot, E)\rangle_{i_R}$. Then Fourier transform is applied to $\widetilde{G}(i_R, E)$ with respect to i_R to get the power spectrum, $|\widetilde{G}(k_y, E)|^2$, in terms of the spatial frequency in y direction. The results of power spectrum $|\widetilde{G}(k_y, E)|^2$ are shown in figure 5 as contour plots for $i_L = 47$ (a) and $i_L = 17$ (b) for a given energy interval. The figure reveals, instead of random patterns, some well-pronounced line segments in the wavevector-energy plane. The line patterns in the power spectrum plot, despite some minor discrepancies, exhibit similar features for the two cases, such as the trend, the starting and ending energy point for each line segment. Furthermore, the line patterns are not continuous, but rather consist of discrete bright spots. That is, when the energy is varied, only for a small set of energy values, there is a dominant frequency (the bright spot), corresponding to pronounced periodic oscillations in the conductance-lead position curve (panels (d)–(f) for figures 2 and 3). While for most other energies, there is no such dominant frequency, indicating random conductance fluctuations versus the right lead position.

Intuitively, since the graphene dot is rectangular, in the vertical direction, the device can be viewed as a ribbon with a finite length. Thus for not-so-small energies, the wavefunction of the quantum dot in the y-direction has a regular waveform. As the right lead moves from bottom to top, when it resides at the local maximum of the probability density function, the transmission would assume a large value. In contrast, when the right lead resides at the local minimum of the probability density function, the modes in the dot and the modes in the right lead cannot couple effectively, leading to a small value of transmission. As a result, the oscillation of the large and small values of transmission follows the regular waveform of the wavefunction. Moreover, since the probability density function is the square of the module of the wavefunction, the frequency of the transmission oscillation should be twice as that of the wavefunction in y direction.

The intuitive understanding can be verified by considering the effect of removing the leads for the quantum dot in figure 1(a), which results in an armchair ribbon of finite length in the vertical direction. We can then calculate the band structure of the corresponding armchair ribbon, assuming that it can be approximated by an infinite ribbon. The width is $L = 20a$. The results are shown in figure 6(a). We then replot figures 5(a) in 6(b) and overlay with the calculated band structure as the crosses (the region indicated by the dashed rectangle in figure 6(a)), with the value of the wavevector being doubled. One can see that the dispersion relation of the armchair ribbon with the doubled wavevector coincides with the line patterns in the wavevector space of conductance variation. This provides direct evidence for the standing-wave-like origin of the oscillation patterns in the conductance curve.

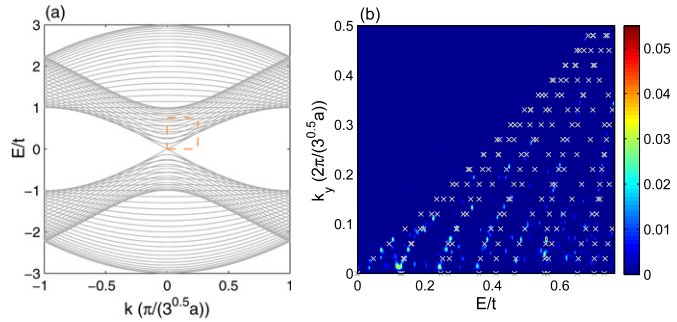

Figure 6. (a) Band structure of armchair graphene ribbon with width $W = 20a$, the same size as the rectangular quantum dot in the x direction. The dashed rectangle indicates the region of band structure shown in (b). (b) Contour plot of the power spectrum in the wavevector k (from i_R) and E/t plane for $i_L = 47$ (the same as in figure 5(a)). The units are arbitrary for the power spectrum. The crosses represent the band structure for the ribbon where the value of the wavevector is doubled.

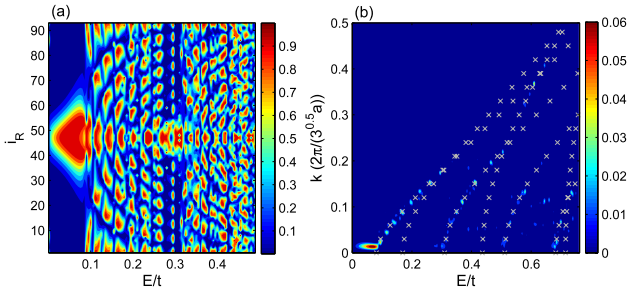

Figure 7. (a) Contour plot of the conductance (in units of $2e^2/h$) as a function of the right lead position i_R and the Fermi energy. (b) Power spectrum of the conductance variation $\widetilde{G}$ in the wavevector k (from i_R) and E/t plane. $L = 10$, $i_L = 47$. The units are arbitrary for the power spectrum.

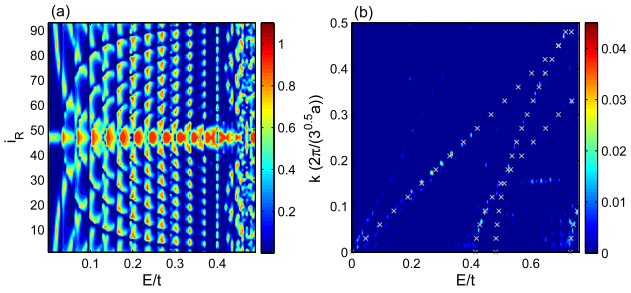

Figure 8. (a) Contour plot of the conductance (in units of $2e^2/h$) as a function of the right lead position i_R and the Fermi energy. (b) Power spectrum of $\widetilde{G}$ in the wavevector k (from i_R) and E/t plane. $L = 5$, $i_L = 47$. The units are arbitrary for the power spectrum.

To further substantiate our numerical observation, we vary the width L of the dot and carry out the same calculations. The results are shown in figure 7 for $L = 10$ and figure 8 for $L = 5$, with the left panel showing the contour plot of the conductance and the right panel showing the corresponding power spectrum in the wavevector space, together with the calculated band structures where the value of the wavevector is doubled. Comparing to figure 4(a), $\widetilde{G}(i_R, E)$ in figures 7(a) and 8(a) exhibit a more regular pattern, and accordingly, the structure in the contour plot of $\widetilde{G}(k, E)$ is also more pronounced. We see again that the power spectrum pattern of the conductance coincides with the calculated band structure for doubled wavevector values.

We now focus on figure 7(b). We see that although the bright spots in the power spectrum $\widetilde{G}(k, E)$ follows the band structure, not all the bands are occupied. For example, as we sweep the energy, the first band ($E/t \sim 0.1$) bears the bright spots of the spectrum of $\widetilde{G}$, indicating its contribution to the conductance. When the second band emerges ($E/t \sim 0.2$), it is not connected with any bright spot, thus this band has no contribution to the conductance oscillation. However, when the third band ($E/t \sim 0.3$) appears, the bright spots jump to this band and the corresponding wavevector restarts from 0 following this band. The fourth band again has no contribution. The fifth band contributes to the conductance oscillation, and so on. Similar selection phenomena of the bands on which the power spectrum scars also holds for other cases, as demonstrated in figures 6(b) and 8(b). While for transmission (conductance) of the corresponding armchair nanoribbon viewed in y direction, it is known that all the bands contribute indistinguishably one mode when energy is above the bottom of the band. Another observation is that, when two bands cross each other, the bright spots can jump from one band to the other (see the two bands around $E/t = 0.4$ in figures 7(b) and 8(b)).

As we shall demonstrate below, this feature can be explained by the dispersion relation and the phase difference of the two sublattices of the wavefunctions. Figure 9(a) shows a contour plot of the energy dispersion relation for graphene, where **K** and **K**′ are the two Dirac points. For a closed device from which both leads are removed (figure 1), in the horizontal (x) direction, the boundary is zigzag but it is armchair in the vertical (y) direction. Figure 9(b) shows the relation between energy and k_y, the y component of the wavevector. Take the **K** point for example, there are two sets of bands for the armchair ribbon. For $E > 0$ the first set is for $k_x > K$, shown in figure 9(b) as the gray (lighter) curves. The other set is for $k_x < K$, shown in figure 9(b) as the red (darker) ones. Regarding the isolated quantum dot as a nanoribbon in the vertical direction, the wavefunction of the armchair ribbon for wavevectors close to the Dirac point **K** has the form [27]

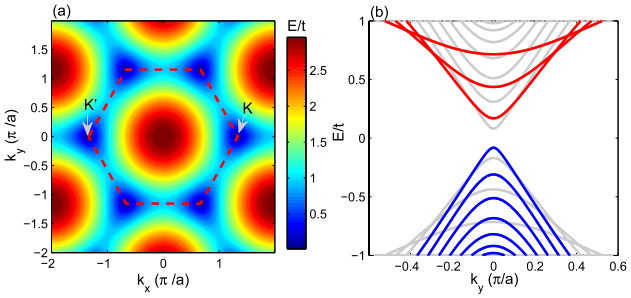

Figure 9. (a) Contour plot of the dispersion relation of graphene with x direction being zigzag. The dashed line indicates the first Brillouin zone. The **K** point is $(4\pi/(3a), 0) = (K, 0)$, and **K**′ point is $(-K, 0)$. (b) Calculated band structure for the armchair nanoribbon with $L = 10$ (corresponding to vertical direction in (a)). For $E > 0$, the gray (lighter) curves are for $k_x > K = 4\pi/(3a)$, the red (darker) ones are for $k_x < K$. For $E < 0$, the gray (lighter) curves are for $k_x < K = 4\pi/(3a)$, the blue (darker) ones are for $k_x > K$. Therefore, for the gray curves, $\text{sign}(k_n/E) = 1$, while for red or blue curves, we have $\text{sign}(k_n/E) = -1$.

$\psi(x, y) = e^{ik_y y}[\phi_A(x), \phi_B(x)]^T$. The Hamiltonian is given by

$$H_{\mathbf{K}} = v_F(\mathbf{p}\cdot\boldsymbol{\sigma}) = v_F\begin{pmatrix} 0 & p_x - ip_y \\ p_x + ip_y & 0 \end{pmatrix},$$

where $\boldsymbol{\sigma}$ denotes the Pauli matrices. The eigen-equation $H\psi = E\psi$ yields

$$v_F\begin{pmatrix} 0 & -i\hbar\partial_x - i\hbar k_y \\ -i\hbar\partial_x + i\hbar k_y & 0 \end{pmatrix}\cdot\begin{pmatrix}\phi_A \\ \phi_B\end{pmatrix} = E\begin{pmatrix}\phi_A \\ \phi_B\end{pmatrix}.$$

The first row yields $v_F(-i\hbar)(\partial_x + k_y)\phi_B(x) = E\phi_A(x)$, or

$$\phi_A(x) = \frac{-i\hbar v_F}{E}(\partial_x + k_y)\phi_B(x). \quad (1)$$

Equivalently, for the second row we have

$$\phi_B(x) = \frac{-i\hbar v_F}{E}(\partial_x - k_y)\phi_A(x). \quad (2)$$

Combining equations (1) and (2), we have $\phi_B(x) = (\hbar^2 v_F^2/E^2)(k_y^2 - \partial_x^2)\phi_B(x)$. Applying the boundary condition of the armchair ribbon, the solution is $\phi_B(x) = Ae^{ik_n x}$, where $k_n = n\pi/L - 4\pi/(3a)$ and L is the width of the ribbon [27]. Substituting this solution back to equation (1), we have

$$\phi_A(x) = \frac{-i\hbar v_F}{E}(ik_n + k_y)\phi_B(x). \quad (3)$$

We now reexamine figure 7(b). The bands can be characterized by their cross points with the energy axis, which are located at the bottom of the bands. In this region, $k_y \approx 0$ and $E \approx v_F\hbar|k_n|$, thus equation (3) becomes

$$\phi_A(x) \approx \frac{\hbar v_F k_n}{E}\phi_B(x) = \text{sign}(k_n/E)\phi_B(x). \quad (4)$$

The same holds for the other Dirac point. We see that, in the region of $k_y \sim 0$, depending on the value of k_n, or the location of k_x (on the right side or the left side of the Dirac point **K**), the wavefunction of A atoms may have the same value or the opposite value as that of B atoms. This has been verified by numerical calculations of the wavefunctions of the armchair ribbons.

It can now be argued that only the bands for which the wavefunctions for A atoms and B atoms possess the same value contribute to the conduction of the quantum dot, while the bands with opposite phases have no contributions. Our idea is to use the mode matching technique in the calculation of the transmission [28]. In particular, the transmission of the quantum dot is nonzero if the modes in the dot match the modes in both left and right leads. The leads are narrow zigzag ribbons. The wavefunctions of A atoms and B atoms are symmetric under reflection with respect to the vertical direction when $E > 0$. Since the leads are narrow and their widths are much smaller than the vertical scale of the quantum dot, the wavefunctions of the dot in the lead region can be regarded as constants. Mode matching is the sum of the cross integral between the wavefunctions of both A and B atoms. If the wavefunctions of A atoms and B atoms have the same value, their contributions add up, resulting in a large transmission. However, if the wavefunctions have the opposite value, the two cross integrals annihilate, leading to nearly zero contribution to the transmission. This explains why the bands with negative k_n, where $k_x < K$ around the **K** point or $k_x > -K$ around the **K**′ point, as shown by the red bands in figure 9(b), do not contribute to conductance and are missing in the power spectrum pattern of $\widetilde{G}$, as shown in figure 7(b).

Note that we have focused on the $E > 0$ case so far. For $E < 0$, we expect the same kind of behavior, i.e., the spectrum of the conductance fluctuation coincides with the dispersion relation. From figure 9(b), for $E > 0$ and $E < 0$ the bands with opposite values are interchanged, thus in the spectrum of the conductance fluctuation, a naive thought would be that the occupied bands will be also interchanged. However, a direct numerical calculation yields the same plots for the conductance and also the spectrum except a reflection from E to $-E$. This can be understood by noting that the bands of the quantum dot with opposite values are interchanged when change from E to $-E$, and a particular state $[\psi_A, \psi_B]$ will change to $[\psi_A, -\psi_B]$ for the dot region. However, the same also happens to the leads. Thus, for $E > 0$, in the leads $\psi_A \approx \psi_B$, only the states with $\psi_A \approx \psi_B$ in the dot region contribute to the conductance. While for $-E$, the wavefunction changes to $[\psi_A, -\psi_B]$ for both leads and the dot. It can be concluded that now the bands with opposite values contribute to the conductance.

Another interesting observation is that in figure 7(a), there is a pronounced triangle-like conductance peak for $E/t < 0.1$. This occurs when the vertical ribbon has a band gap. To be specific, the vertical ribbon without the leads is an armchair ribbon. Depending on the width of the ribbon, e.g., when number of atoms in a repeating slice is $N = 4n + 2$, $n = 3m - 1$ ($m = 1, 2, \ldots$ is an integer), the valence band and the conductance band could cross each other where the ribbon behaves metallic. For other n values, the ribbon has a gap, which is inversely proportional to the width of the ribbon. The profile of this conductance peak reveals a transition from the localized state at the zigzag edge for low

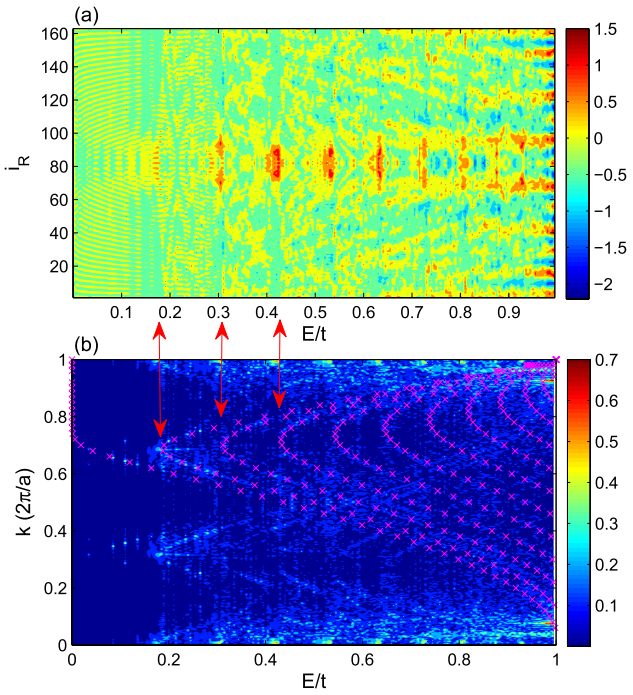

Figure 10. (a) Contour plot of the conductance variation $\widetilde{G}$ (in units of $2e^2/h$) as a function of the right lead position i_R and the Fermi energy. (b) The power spectrum of $\widetilde{G}$ in the wavevector k (from i_R) and E/t plane. The crosses indicate the band structure of the corresponding zigzag ribbon. $N = 4 \times 170 + 2 = 682$. $L = 12$, $i_L = 82$. The units are arbitrary for the power spectrum.

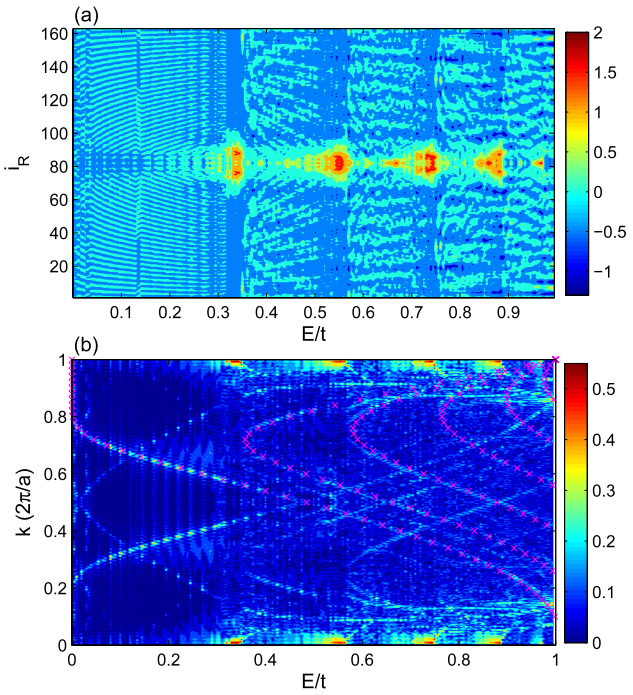

Figure 11. (a) Contour plot of the conductance variation $\widetilde{G}$ in the right lead position i_R and the Fermi energy E/t plane. (b) The power spectrum of the transmission shown in (a) in the wavevector k (from i_R) and E/t plane. The crosses indicate the band structure of the corresponding zigzag ribbon. $N = 4 \times 170 + 2 = 682$. $L = 6$, $i_L = 82$. The units are arbitrary for the power spectrum.

energy ($E \sim 0.01t$) to the first extended state of the first band ($E \sim 0.09t$). The former does not contribute to transmission, while the latter does. Since the ribbon is narrow, there are no other intermediate states between these two states. As the energy is increased, the extended state at ($E \sim 0.09t$) plays a more dominant role, leading to a larger i_R interval for high transmission.

4. Systems with armchair horizontal boundaries

The numerical results and analysis presented so far are with respect to graphene quantum dots with horizontal zigzag boundaries. For graphene quantum dots with armchair horizontal boundaries, as shown in figure 1(b), the conductance properties appear distinctly from those associated with the zigzag horizontal boundary systems. For comparison, we calculate the conductance for an armchair quantum dot with a similar size as the one used for figures 2–6. The leads also support a maximum of 8 transmission modes. Since the conductance increases with the energy, to grasp the conductance variation as the right lead moves, for each energy E we calculate conductance variation $\widetilde{G}(i_R, E) = G(i_R, E) - \langle G(\cdot, E)\rangle_{i_R}$, and plot this $\widetilde{G}$ in figure 10(a). Comparing with the patterns shown in figure 4, we see that the conductance fluctuation patterns are different. For the zigzag quantum dot, at small energies, the spatial wavelength of the conductance fluctuation over the right lead position is long. But for the armchair dot, even at small energies, the spatial wavelength of the conductance fluctuation is still short. A common feature, however, is that the conductance pattern is also divided into several different sub-energy levels. As in the zigzag case, this is originated from the standing-wave-like wavefunctions and, consequently, the power spectrum of the conductance variation would follow the band structure of the corresponding ribbon looking in the vertical direction. We have carried out Fourier transform of $\widetilde{G}$ in the i_R dimension, and plotted the power spectrum in figure 10(b). Comparing the two subplots, we see that, as the energy increases, whenever it crosses a band as shown in figure 10(b), the conductance fluctuation pattern in figure 10(a) will exhibit a drastic change, such as for $E/t \sim 0.2, 0.3, 0.4$ etc, as indicated by the arrows. We have overlaid the bands of the corresponding vertical ribbon, where the value of the wavevector is doubled. The bright spots of the power spectrum follow the band structure well. In this case, when energy approaches zero, from the dispersion relation the wavevector is not approaching zero as in the zigzag dot case, but has a limit value of $K/2 = 2\pi/(3a)$. The wavelength ($\sim 1/k$) of the wavefunction in the vertical direction of the quantum dot is consequently short, leading to rapid conductance oscillations.

To verify the generality of the above observation of the conductance oscillation/fluctuation pattern in the armchair quantum dots, we have carried out parallel computations for shorter quantum dots as in the zigzag cases. The results are shown in figure 11 for $L = 6$ and figure 12 for $L = 3$. As in the zigzag cases, narrow dots support fewer transverse modes and exhibit more coherent transmissions, and regular conductance oscillation patterns are thus more frequent.

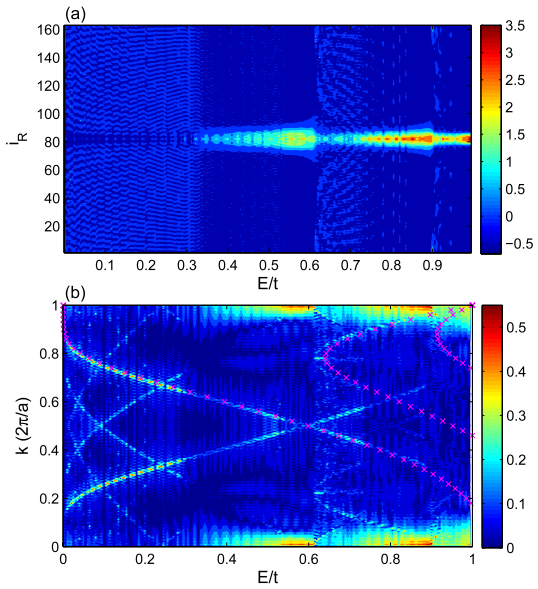

Figure 12. (a) Contour plot of the conductance variation $\widetilde{G}$ in the $i_R - E/t$ plane. (b) The power spectrum of $\widetilde{G}$ shown in (a) in the wavevector k (from i_R) and E/t plane. The crosses indicate the band structure of the corresponding zigzag ribbon. $N = 4 \times 170 + 2 = 682$. $L = 3$, $i_L = 82$. The units are arbitrary for the power spectrum.

The coincidence of the power spectrum pattern and the band structure for all the three armchair quantum dots validates the standing-wave conjecture as in the zigzag dot cases.

5. Conclusion

In conclusion, we have investigated the effect of lead positions on conductance oscillation/fluctuations in rectangular graphene quantum dots. We have provided systematic computational results and a physical theory for both zigzag and armchair horizontal boundaries. Our main finding is that the conductance oscillation/fluctuations are originated from the standing-wave patterns of the wavefunctions in the quantum dot, an effect of quantum interference. This is established by the consistency of the power spectrum analysis of the conductance variation and the energy-band structure of the underlying quantum dot when viewed as a ribbon in the vertical direction. For the armchair horizontal boundaries, all the bands are occupied by the power spectrum of the conductance variation. While for the case of zigzag horizontal boundaries, some bands are missing. The selection of the bands on which the conductance fluctuation scars is determined by the relative phase of the wavefunction for the two atoms in a unit cell, where only those with the same phase in the case of $E > 0$ have contributions. Note that our observation is general that it happens whenever the lead is small compared to the scale of the dot, and the value of the wavefunction at the edge of the dot has sensitive dependence on the location. We anticipate these results to be useful in the design and development of future graphene-based nanoscale electronic circuits, where dot structure and point contacts are fundamental elements.

Acknowledgments

This work was supported by AFOSR under Grant No. FA9550-12-1-0095 and by ONR under Grant No. N00014-08-1-0627. LH was also supported by NSFC under Grant No. 11005053 and by the Fundamental Research Funds for the Central Universities under Grant No. Izujbky-2012-19.

References

[1] Novoselov K S *et al* 2004 *Science* **306** 666
Novoselov K S *et al* 2005 *Nature* **438** 197
Avouris P, Chen Z and Perebeinos V 2007 *Nature Nanotechnol.* **2** 605
Geim A K and Novoselov K S 2007 *Nature Mater.* **6** 183
Beenakker C W J 2008 *Rev. Mod. Phys.* **80** 1337
Castro Neto A H, Guinea F, Peres N M R, Novoselov K S and Geim A K 2009 *Rev. Mod. Phys.* **81** 109
Geim A K 2009 *Science* **324** 1530–4
[2] Bolotin K I *et al* 2008 *Solid State Commun.* **146** 351
[3] Huard B *et al* 2007 *Phys. Rev. Lett.* **98** 236803
Özyilmaz B *et al* 2007 *Phys. Rev. Lett.* **99** 166804
Zhang L M and Fogler M M 2008 *Phys. Rev. Lett.* **100** 116804
Williams J R, DiCarlo L and Marcus C M 2007 *Science* **317** 638
Berger C *et al* 2006 *Science* **26** 1191
Lemme M C, Echtermeyer T J, Baus M and Kurz H 2007 *IEEE Electron Device Lett.* **28** 282
[4] Yazyev O V and Katsnelson M I 2008 *Phys. Rev. Lett.* **100** 047209
[5] Watcharotone S *et al* 2007 *Nano Lett.* **7** 1888–92
[6] Xia F, Mueller T, Lin Y-m, Valdes-Garcia A and Avouris P 2009 *Nature Nanotechnol.* **4** 839–43
[7] Dan Y, Lu Y, Kybert N J, Luo Z and Johnson A T C 2009 *Nano Lett.* **9** 1472–5
[8] Postma H W Ch 2010 *Nano Lett.* **10** 420–5
[9] Mohanty N and Berry V 2008 *Nano Lett.* **8** 4469–76
[10] Cohen-Karni T, Qing Q, Li Q, Fang Y and Lieber C M 2010 *Nano Lett.* **10** 1098–102
[11] Bunch J S, Yaish Y, Brink M, Bolotin K and McEuen P L 2005 *Nano Lett.* **5** 287–90
[12] Ujiie Y *et al* 2009 *J. Phys.: Condens. Matter* **21** 382202
[13] Krsti V *et al* 2008 *Nano Lett.* **8** 1700–3
[14] Yu Y-J, Zhao Y, Ryu S, Brus L E, Kim S and Kim P 2009 *Nano Lett.* **9** 3430–4
[15] Lee E J H, Balasubramanian K, Weitz R T, Burghard M and Kern K 2008 *Nature Nanotechnol.* **3** 486–90
[16] Yang R, Huang L, Lai Y-C and Grebogi C 2011 *Europhys. Lett.* **94** 40004
[17] Liang G, Neophytou N, Lundstrom M S and Nikonov D E 2008 *Nano Lett.* **8** 1819–24
Wang Q J and Che J G 2009 *Phys. Rev. Lett.* **103** 066802
Barraza-Lopez S, Vanević M, Kindermann M and Chou M Y 2010 *Phys. Rev. Lett.* **104** 076807
[18] Takagaki Y and Ploog K H 1998 *Phys. Rev.* B **57** R12689–92
[19] Katsnelson M I and Guinea F 2008 *Phys. Rev.* B **78** 075417
[20] Kechedzhi K, Kashuba O and Fal'ko V I 2008 *Phys. Rev.* B **77** 193403
[21] Huang L, Yang R and Lai Y-C 2011 *Europhys. Lett.* **94** 58003
[22] González J W, Pacheco M, Rosales L and Orellana P A 2011 *Phys. Rev.* B **83** 155450

[23] Bird J P *et al* 1999 *Phys. Rev. Lett.* **82** 4691
[24] See, for example, Imry Y 1986 *Europhys. Lett.* **1** 249
Lee P A, Stone A D and Fukuyama H 1987 *Phys. Rev.* B **35** 1039
Ketzmerick R 1996 *Phys. Rev.* B **54** 10841
Jalabert R A, Baranger H U and Stone A D 1990 *Phys. Rev. Lett.* **65** 2442
Prigodin V N, Efetov K B and Iida S 1993 *Phys. Rev. Lett.* **71** 1230
Sachrajda A S *et al* 1998 *Phys. Rev. Lett.* **80** 1948
[25] Datta S 1995 *Electronic Transport in Mesoscopic Systems* (Cambridge: Cambridge University Press)
[26] Huang L, Lai Y-C, Ferry D K, Akis R and Goodnick S M 2009 *J. Phys.: Condens. Matter* **21** 344203
[27] Brey L and Fertig H A 2006 *Phys. Rev.* B **73** 235411
[28] Ferry D K, Goodnick S M and Bird J 1997 *Transport in Nanostructures* (New York: Cambridge University Press)